

# Transport Upscaling Using Multi-Rate Mass Transfer in Three-Dimensional Highly Heterogeneous Porous Media

Liangping Li<sup>a,b,\*</sup>, Haiyan Zhou<sup>a,b</sup>, J. Jaime Gómez-Hernández<sup>b</sup>

<sup>a</sup>*School of Water Resources and Environment, China University of Geosciences(Beijing), China*

<sup>b</sup>*Group of Hydrogeology, Universitat Politècnica de València, Spain*

---

## Abstract

A methodology for transport upscaling of three-dimensional highly heterogeneous formations is developed and demonstrated. The overall approach requires a prior hydraulic conductivity upscaling using an interblock-centered full-tensor Laplacian-with-skin method followed by transport upscaling. The coarse scale transport equation includes a multi-rate mass transfer term to compensate for the loss of heterogeneity inherent to all upscaling processes. The upscaling procedures for flow and transport are described in detail and then applied to a three-dimensional highly heterogeneous synthetic example. The proposed approach not only reproduces flow and transport at the coarse scale, but it also reproduces the uncertainty associated with the predictions as measured by the ensemble variability of the breakthrough curves.

*Keywords:* upscaling, heterogeneity, solute transport, mass transfer

---

## 1. Introduction

Upscaling flow and transport has been disregarded by some on the basis that it is not needed because our computers are capable of handling larger and larger numerical models. However, we know by experience that there will always be a discrepancy between the scale at which we can characterize the medium, and the scale at which we can run our numerical codes. This discrepancy renders upscaling necessary in order to transfer the information collected at the measurement scale into a coarser scale better suited for numerical modeling.

In the last decades, many reviews have been published dealing with upscaling but mostly focusing on hydraulic conductivity upscaling [e.g., 57, 41, 48]. In comparison with the effort devoted to the upscaling of hydraulic conductivity, less attention has been paid to upscaling for solute transport modeling. For

---

\*Corresponding author

*Email addresses:* [liali@upvnet.upv.es](mailto:liali@upvnet.upv.es) (Liangping Li), [haizh@upvnet.upv.es](mailto:haizh@upvnet.upv.es) (Haiyan Zhou), [jaimedihma.upv.es](mailto:jaimedihma.upv.es) (J. Jaime Gómez-Hernández)

11 example, Dagan [11] noted that hydraulic conductivity upscaling induces a loss of information and advised  
12 to compensate for this loss by splitting the solute plume into subplumes with effective dispersivities derived  
13 from stochastic theory. Rubin et al. [44] developed an upscaling method to derive effective block-scale  
14 dispersivities using a perturbation method, which accounts for the loss of subgrid variability in the upscaled  
15 numerical model. These two approaches are based on analytical techniques, which have a limited range  
16 of application because of their underlying assumptions. Numerical methods, on the contrary, are more  
17 general, since they are not restricted by the geometry of the domain, the type of boundary conditions, or the  
18 degree of heterogeneity. Scheibe and Yabusaki [49] examined the impact of hydraulic conductivity upscaling  
19 using the power-averaging method with different exponents [33]. They found that although flows and heads  
20 can be preserved after upscaling the hydraulic conductivities, the discrepancy on transport predictions is  
21 substantial. Cassiraga et al. [7] applied the simple-Laplacian technique [57] to upscale hydraulic conductivity  
22 and evaluated the impact of upscaling on solute transport for various degrees of heterogeneous media in  
23 two dimensions. They concluded that the prediction of solute transport at the coarser scale will provide  
24 reasonably good estimates of the early particle arrival times but will largely underestimate the late travel  
25 times; the explanation for this behavior was the existence and connectedness of extreme-valued hydraulic  
26 conductivities at the fine scale, which are lost after upscaling. To overcome this inability, Fernàndez-García  
27 and Gómez-Hernández [16] extended this study and introduced an enhanced block dispersion tensor to  
28 compensate for the loss of information. They found that, with this approach the median travel time could  
29 be reproduced but that the tails of the breakthrough curves were largely underestimated. They suggested  
30 that a mass transfer process should be introduced at the coarse scale to make up for the information at the  
31 small scale that cannot be resolved by the upscaled model in heterogenous media. Fernàndez-García et al.  
32 [18] examined the use of a mass transfer process with different memory functions as part of the constitutive  
33 transport equation at the coarse scale, in conjunction with hydraulic conductivity upscaling with the simple-  
34 Laplacian technique in 2D. The results showed that considering a double-rate or a truncated power-law mass  
35 transfer model at the coarse scale was enough to properly describe the ensemble average behavior of the main  
36 features associated with the breakthrough curves. However, the uncertainty associated with the predictions  
37 is underestimated after upscaling due to the lack of memory in space during the upscaling process.

38 It is important to note that the use of a mass transfer process as part of the constitutive equation for  
39 transport at the coarse scale model has also been proposed by Guswa and Freyberg [26], Zinn and Harvey  
40 [64], Willmann et al. [59] and Frippiat and Holeyman [20]. However, these studies mainly focus on upscaling  
41 up to a completely homogeneous aquifer. Guswa and Freyberg [26] conclude that a mass exchange term

42 is needed only if the equivalent hydraulic conductivity is larger than the geometric mean of the underlying  
 43 conductivity field, Zinn and Harvey [64] suggest that a mass exchange is necessary and conclude that the  
 44 multi-rate model should better compensate for the loss of resolution than the single-rate model, and later  
 45 Fernàndez-Garcia et al. [18] demonstrated that, indeed, the double-rate model and the power-law mass  
 46 transfer model outperform the single-rate model for upscaling purposes.

47 In the current work, we extend to 3D the study by Fernàndez-Garcia et al. [18], who proposed a transport  
 48 upscaling method using a multi-rate mass transfer. We also introduce an elaborated interblock Laplacian-  
 49 with-skin hydraulic conductivity upscaling approach, for optimal reproduction of the flows at the coarse scale.  
 50 Although the extension of the methodology to three-dimensions may appear as conceptually straightforward,  
 51 we have found that it is necessary to make some adjustments to efficiently reproduce the breakthrough curves.  
 52 Additionally, unlike most studies that focused primarily on a single realization analysis, the present study  
 53 analyzes the upscaling at the ensemble level in order to analyze also how prediction uncertainty upscales.

54 The outline of this paper is as follows. We first introduce the flow and transport governing equations  
 55 at two different support scales. Next, the importance of using an interblock Laplacian-with-skin hydraulic  
 56 conductivity upscaling is illustrated, with emphasis on the numerical implementation in three-dimensions.  
 57 We then describe the transport upscaling with mass transfer in two dimensions and discuss the modifications  
 58 of the method for its application in three-dimensions. Finally, numerical tests demonstrate the accuracy and  
 59 efficiency of the method. We end with a discussion on the weaknesses and strengths of the proposed approach,  
 60 with an indication of avenues for improvement.

## 61 **2. Methodology**

### 62 *2.1. Background*

#### 63 *2.1.1. Fine scale equations*

64 At the fine scale, denoted herein by the superscript  $f$ , under steady-state flow conditions and in the  
 65 absence of sinks and sources, the flow equation of an incompressible fluid in saturated porous media in a  
 66 Cartesian coordinate system can be obtained by combining the continuity equation and Darcy's law [1]:

$$\nabla \cdot [\mathbf{K}^f(\mathbf{x}^f) \nabla h^f(\mathbf{x}^f)] = 0 \quad (1)$$

67 where  $h^f [L]$  is the piezometric head;  $\mathbf{K}^f [LT^{-1}]$  is a symmetric positive-definite rank-two tensor;  $\mathbf{x}^f$  represents  
 68 the fine scale coordinates.

69 Similarly, using the solute mass conservation equation and assuming that Fick's law is appropriate at the  
70 local scale, the three-dimensional advective-dispersive equation (ADE) for solute transport is often written  
71 as [19]:

$$\phi^f \frac{\partial C^f(\mathbf{x}^f, t)}{\partial t} = -\nabla \cdot [\mathbf{q}^f(\mathbf{x}^f) C^f(\mathbf{x}^f, t)] + \nabla \cdot [\phi^f \mathbf{D}^f \nabla C^f(\mathbf{x}^f, t)] \quad (2)$$

72 where  $C^f [ML^{-3}]$  is the dissolved concentration of solute in the liquid phase;  $\phi^f$  [dimensionless] is the porosity;  
73  $\mathbf{q}^f [LT^{-1}]$  is the Darcy velocity given by  $\mathbf{q}^f(\mathbf{x}) = -\mathbf{K}^f(\mathbf{x}) \nabla h^f(\mathbf{x})$ ;  $\mathbf{D}^f [L^2 T^{-1}]$  is the local hydrodynamic  
74 dispersion coefficient tensor with eigenvalues (associated with the principal axes, which are parallel and  
75 perpendicular to the direction of flow) given by [5]:

$$D_i^f = D_m + \alpha_i \frac{|\mathbf{q}^f|}{\phi^f} \quad (3)$$

76 where  $\alpha_i$  are the local dispersivity coefficients, more specifically,  $\alpha_L, \alpha_T^H$  and  $\alpha_T^V$  are, respectively, the lon-  
77 gitudinal dispersivity coefficient and the transverse dispersivity coefficient in the directions parallel and  
78 orthogonal to flow, and  $D_m$  is the effective molecular diffusion coefficient.

79 The fine scale transport equation (2) is only valid if the Fickian assumption is satisfied at the small scale.  
80 Here, we assume that the ADE is capable of reproducing the tracer spreading at the fine scale. Salamon  
81 et al. [47] at the MADE site and Riva et al. [42] at the Lauswiesen site have shown that for cases in which,  
82 apparently, the transport spreading does not look Fickian at the macroscopic scale, the ADE equation is  
83 applicable if the small-scale variability of hydraulic conductivity is properly modeled at the smallest scale  
84 possible.

### 85 2.1.2. Coarse scale equations

86 There are two main approaches to get the coarse scale equations. On one hand, those who work analyt-  
87 ically from the fine scale equations and apply regularization techniques to derive the equations that would  
88 express the state of the system on a larger scale. Examples of these works can be found in [9, 39, 32, 25].  
89 On the other hand, those who empirically postulate the coarse scale expression (after the fine scale one) and  
90 then try to determine the parameter values of the postulated coarse scale expressions. Examples of these  
91 works can be found in [43, 24, 23, 26]. In the first approach, the authors generally obtain equations which are  
92 nonlocal, that is, the parameters associated to a given block at the coarse scale depend not only on the fine  
93 scale parameters values within the block, but also on the values outside the block. This fact is recognized  
94 by some authors using the second approach when the coarse block parameters are computed on local flow

95 and/or transport models which extend beyond size of the block being upscaled, so that the influence of the  
 96 nearby cells is captured [57]. We have opted, in this paper, for the second approach.

97 At the coarse scale, denoted herein by the superscript  $c$ , the flow equation is taken to have the same  
 98 expression as the fine scale equation, but with  $\mathbf{K}^f$  replaced by an upscaled hydraulic conductivity tensor  $\mathbf{K}^c$ :

$$\nabla \cdot [\mathbf{K}^c(\mathbf{x}^c) \nabla h^c(\mathbf{x}^c)] = 0 \quad (4)$$

99 where  $h^c[L]$  designates the coarse scale piezometric head, and  $\mathbf{x}^c$  refers to the coarse scale coordinates.

100 In earlier studies of transport at the coarse scale, only upscaling of the flow controlling parameters was  
 101 performed [e.g., 49, 7, 37]. That is, upscaled  $\mathbf{K}^c$  values were derived, and the same advection dispersion  
 102 equation was used both at the fine and coarse scales. However, recent findings have demonstrated that  
 103 the transport equation to be used at the coarse scale should include an enhanced dispersion tensor and a  
 104 fictitious mass exchange process as a proxy to represent the mass transfer processes taking place within the  
 105 coarse block and largely associated with the within-block heterogeneity [e.g., 64, 16, 59, 18].

106 We have chosen the multi-rate mass transfer model (MRMT) [27, 6] as the mass exchange expression to  
 107 be used at the coarse scale. Alternative models such as the continuous time random walk [3] or fractional  
 108 derivatives [2] could be used as well. Fernàndez-Garcia et al. [18] discussed the use of the MRMT for upscaling  
 109 purposes in 2D, and its versatility to treat complex heterogeneities; furthermore, it was successfully applied  
 110 at the MADE aquifer by Feehley et al. [15] and at the Lauswiesen site by Riva et al. [42]. Many transport  
 111 codes based on the MRMT model [e.g., 61, 6, 45, 50] indicate the great potential of this approach.

112 The upscaled transport equation, including the MRMT model, can be described by the following governing  
 113 equation [27, 6]:

$$\phi_m^c \frac{\partial C_m^c(\mathbf{x}^c, t)}{\partial t} = -\nabla \cdot [\mathbf{q}^c(\mathbf{x}^c) C_m^c(\mathbf{x}^c, t)] + \nabla \cdot [\phi_m^c \mathbf{D}^c \nabla C_m^c(\mathbf{x}^c, t)] - \phi_m^c \Gamma(\mathbf{x}^c, t) \quad (5)$$

114 where  $\phi_m^c$  [dimensionless] defines the pore volume fraction of the mobile domain;  $C_m^c[ML^{-3}]$  is the solute  
 115 concentration in the mobile region of the coarse block;  $\mathbf{q}^c[LT^{-1}]$  is the Darcy velocity derived from the  
 116 upscaled hydraulic conductivity;  $\mathbf{D}^c[L^2T^{-1}]$  is an enhanced block dispersion tensor, which includes the fine  
 117 scale local hydrodynamic dispersion ( $\alpha_i$ ) and a macrodispersivity term ( $A_i$ ) [16, 18]:

$$D_i^c = D_m + (\alpha_i + A_i) \frac{|\mathbf{q}^c|}{\phi_m^c} \quad (6)$$

118 where  $D_i^c$  are the eigenvalues of  $\mathbf{D}^c$  associated with the principal axes, which are parallel and perpendicular

119 to the flow direction. The additional mass exchange term  $\Gamma(\mathbf{x}^c, t)$  [ $ML^{-3}T^{-1}$ ] can be expressed in terms of  
 120 mobile concentrations by using a convolution product with a memory function  $g(\mathbf{x}^c, t)$  [ $T^{-1}$ ] [6, 28]:

$$\begin{aligned}\Gamma(\mathbf{x}^c, t) &= \beta(\mathbf{x}^c) \int_0^t g(\mathbf{x}^c, \tau) \frac{\partial C_m^c(\mathbf{x}^c, t - \tau)}{\partial \tau} d\tau \\ g(\mathbf{x}^c, t) &= \int_0^\infty \alpha f(\mathbf{x}^c, \alpha) e^{-\alpha t} d\alpha\end{aligned}\tag{7}$$

121 where  $\beta(\mathbf{x}^c)$  [dimensionless] is the so-called capacity ratio;  $\alpha$  [ $T^{-1}$ ] is a continuous positive variable repre-  
 122 senting the multiple mass transfer rate coefficients, and  $f(\mathbf{x}^c, \alpha)$  [ $T$ ] denotes the probability density function  
 123 of the mass transfer rate coefficients. Therefore, once  $f(\mathbf{x}^c, \alpha)$  is given, the MRMT model equation (5) can  
 124 be numerically solved. It is worth emphasizing that, the macrodispersivity term  $A_i$  and the mass transfer  
 125 model are introduced as fictitious processes to make up for the presence of low and high conductivity zones  
 126 which are smeared out after upscaling, and for the diffusive-like process occurring within the coarse block  
 127 due to the heterogeneity. In this respect, it is consistent with Zinn and Harvey [64], Willmann et al. [59],  
 128 and Riva et al. [42] who used the MRMT model to account for the subgrid heterogeneity in the upscaled  
 129 transport model.

## 130 2.2. Hydraulic conductivity upscaling using the Laplacian-with-skin method

131 In contrast with the previous studies by Fernàndez-Garcia and Gómez-Hernández [16] and Fernàndez-  
 132 Garcia et al. [18] that used the simple-Laplacian scheme to compute the block equivalent conductivities in two  
 133 dimensions, here, we use a more sophisticated interblock Laplacian-with-skin three-dimensional full-tensor  
 134 hydraulic conductivity upscaling technique, which is an extension of an earlier two-dimensional approach  
 135 [21]. In essence, the Laplacian-with-skin upscaling scheme is an improved version of the simple-Laplacian  
 136 approach. With regard to the simple-Laplacian method, Li et al. [37] have already demonstrated that it  
 137 fails to reproduce interblock flow at the coarse scale and further underestimates contaminant spread at the  
 138 MADE site. The major disadvantage of the simple-Laplacian approach is the assumption that the upscaled  
 139 conductivity tensor is diagonal. For the details on the different upscaling processes, the reader is referred to  
 140 the work by Wen and Gómez-Hernández [57], or more recently by Li et al. [37].

141 Gómez-Hernández [21] presented the Laplacian-with-skin approach recognizing the nonlocal nature of  
 142 the upscaled conductivity tensor. The skin (a ring of cells surrounding the block) is used to approximate the  
 143 actual boundary conditions around the block being upscaled without having to solve the flow problem for  
 144 the entire aquifer (as previous authors had done, i.e., White and Horne [58]). For each block being upscaled,  
 145 the algorithm consists of three steps: (a) isolate the block, plus a surrounding ring of cells (referred to as the

146 skin), and solve a local flow problem numerically for a set of boundary conditions inducing fluxes in different  
147 directions across the block; (b) for each boundary condition the spatially-averaged flow and gradient within  
148 the block are calculated; (c) and then, the components of the upscaled hydraulic conductivity tensor are  
149 determined by solving the following overdetermined system of linear equations by a standard least squares  
150 procedure:

$$\begin{bmatrix}
\langle \partial h / \partial x \rangle_1 & \langle \partial h / \partial y \rangle_1 & \langle \partial h / \partial z \rangle_1 & 0 & 0 & 0 \\
0 & \langle \partial h / \partial x \rangle_1 & 0 & \langle \partial h / \partial y \rangle_1 & \langle \partial h / \partial z \rangle_1 & 0 \\
0 & 0 & \langle \partial h / \partial x \rangle_1 & 0 & \langle \partial h / \partial y \rangle_1 & \langle \partial h / \partial z \rangle_1 \\
\langle \partial h / \partial x \rangle_2 & \langle \partial h / \partial y \rangle_2 & \langle \partial h / \partial z \rangle_2 & 0 & 0 & 0 \\
0 & \langle \partial h / \partial x \rangle_2 & 0 & \langle \partial h / \partial y \rangle_2 & \langle \partial h / \partial z \rangle_2 & 0 \\
0 & 0 & \langle \partial h / \partial x \rangle_2 & 0 & \langle \partial h / \partial y \rangle_2 & \langle \partial h / \partial z \rangle_2 \\
\dots & \dots & \dots & \dots & \dots & \dots \\
\langle \partial h / \partial x \rangle_n & \langle \partial h / \partial y \rangle_n & \langle \partial h / \partial z \rangle_n & 0 & 0 & 0 \\
0 & \langle \partial h / \partial x \rangle_n & 0 & \langle \partial h / \partial y \rangle_n & \langle \partial h / \partial z \rangle_n & 0 \\
0 & 0 & \langle \partial h / \partial x \rangle_n & 0 & \langle \partial h / \partial y \rangle_n & \langle \partial h / \partial z \rangle_n
\end{bmatrix} \cdot \begin{bmatrix} K_{xx}^c \\ K_{xy}^c \\ K_{xz}^c \\ K_{yy}^c \\ K_{yz}^c \\ K_{zz}^c \end{bmatrix} = - \begin{bmatrix} \langle q_x \rangle_1 \\ \langle q_y \rangle_1 \\ \langle q_z \rangle_1 \\ \langle q_x \rangle_2 \\ \langle q_y \rangle_2 \\ \langle q_z \rangle_2 \\ \dots \\ \langle q_x \rangle_n \\ \langle q_y \rangle_n \\ \langle q_z \rangle_n \end{bmatrix} \quad (8)$$

151 where  $q_x$   $q_y$   $q_z$  are the components of the Darcy flux  $\mathbf{q}$  obtained from the local solution of the flow equation;  
152 angle brackets indicate spatial averaging within the block; subscript  $n$  denotes an index referring to the  
153 different boundary conditions;  $K_{xx}^c \dots K_{zz}^c$  are the components of the upscaled equivalent conductivity  $\mathbf{K}^c$ .  
154 Note that the requirement of symmetry is enforced implicitly [62] in this system of equations.

155 Although we are aware of the works by Zijl and Stam [63] and Bierkens and Gaast [4] in which they  
156 argue that the upscaled conductivity tensor may be non-symmetric, we prefer to maintain symmetry at the  
157 block level to preserve its physical meaning: that opposite gradient vectors should induce opposite specific  
158 discharge vectors. Likewise, we enforce positive definiteness, since it is non-physical that the scalar product  
159 of the gradient vector and the specific discharge be positive (flow never goes upgradient). However, the  
160 approach would be equally applicable without imposing symmetry on the upscaled conductivity tensor.

161 Since we plan to solve the flow equation by finite differences, a further improvement in the hydraulic con-  
162 ductivity upscaling consists in computing the upscaled hydraulic conductivity tensors at the block interfaces  
163 rather than at block centers. This is done by isolating an aquifer volume centered at the interface, plus a skin,  
164 prior to solving the local flow problem [62]. In fact, this suggestion of an upscaled hydraulic conductivity  
165 based on the interface agrees with the works of Chen et al. [8], Wen et al. [55], and He and Durlofsky [31],

166 who already pointed out that the upscaling of transmissibility (the equivalent to interblock conductivity in  
 167 petroleum engineering) provided a more accurate coarse scale result than permeability upscaling.

### 168 2.3. Transport upscaling using mass transfer

169 Both in petroleum engineering and in subsurface hydrogeology, many studies have demonstrated that  
 170 hydraulic conductivity upscaling is not enough to reproduce transport at the coarse scale [e.g., 49, 8, 16].  
 171 We have adopted the method proposed by Fernández-García et al. [18] to address this problem, whereby  
 172 the coarse scale transport equation includes a mass transfer term to compensate for the loss of information  
 173 at the coarse scale. The problem we face is replacing a heterogeneous block within which the heterogeneity  
 174 induces solute dispersion by a homogeneous block with enhanced dispersion and an associated multi-rate  
 175 mass transfer process, the parameters of which have to be determined to induce the same solute dispersion  
 176 induced by the within block heterogeneity. To this extent mass transport is solved at the fine scale using a  
 177 particle tracking random walk approach and the residence times of the particles within the block are computed  
 178 resulting in a cumulative distribution of residence times  $F_\tau(\tau)$ . The objective of transport upscaling is to  
 179 determine the multi-rate mass transfer parameter resulting in the same residence time distribution. This  
 180 is accomplished by a curve fitting process making use of an approximate solution for the residence time  
 181 distribution of the multi-rate mass transfer transport equation in 1D,  $F_\tau^*(\tau)$ . The Laplacian transform of  
 182  $F_\tau^*(\tau)$  is given by [29, 18]:

$$\tilde{F}_\tau^*(p) \approx \frac{1}{p} \exp \left[ L_b \left( \frac{v_m}{2D_\ell^c} - \sqrt{\frac{v_m^2}{4D_\ell^{c2}} + \frac{\tilde{\psi}(p)}{D_\ell^c}} \right) \right] \quad (9)$$

183 where  $L_b[L]$  is the mean travel displacement of solute mass particles; the mobile velocity  $v_m[LT^{-1}]$  is defined  
 184 by:

$$v_m = \frac{\|\mathbf{q}^c\|}{\phi_m^c} \quad \phi_m^c = \frac{\phi_e^c}{1 + \beta} \quad (10)$$

185 and  $\tilde{\psi}(p)$  is defined by:

$$\tilde{\psi}(p) = p + \beta \int_0^\infty f(\alpha) \frac{p\alpha}{p + \alpha} d\alpha \quad (11)$$

186  $p$  is the Laplace transform variable;  $f(\alpha)$  is the density function given in terms of the mass transfer coefficients,  
 187 the expression of which depends on the multi-rate process considered. For instance, for the case of the double-  
 188 rate mass transfer process it is:

$$f(\alpha) = \frac{\beta_1}{\beta} \delta(\alpha - \alpha_1) + \frac{\beta_2}{\beta} \delta(\alpha - \alpha_2) \quad (12)$$



189 with

$$\beta_1 + \beta_2 = \beta \quad (13)$$

190 where  $\beta_1$  and  $\beta_2$  [dimensionless] are the capacities of each immobile phase;  $\alpha_1$  and  $\alpha_2$  [ $T^{-1}$ ] are the transfer  
 191 rates in each immobile phase and  $\delta(\cdot)$  is the Dirac delta.

192 We also found that, in order to preserve the mean travel time of the plume to each control plane, it was  
 193 not enough to match the particle residence time distributions for each block but that it was necessary to  
 194 make a local upscaling of the effective porosity. For our purpose it was sufficient to define a coarse scale  
 195 effective porosity  $\phi_e^c$  [dimensionless] piecewise in between each pair of control planes as follows:

$$\phi_{e,i}^c = \frac{\bar{\tau}_{cp,i}^f - \bar{\tau}_{cp,i-1}^f}{\bar{\tau}_{cp,i}^c - \bar{\tau}_{cp,i-1}^c} \quad i = 1, 2 \dots n_{cp} \quad (14)$$

196 where  $\bar{\tau}_{cp,i}^f$  is the mean travel time at the  $i$  control plane computed at the fine scale with porosity  $\phi_f$ ;  $\bar{\tau}_{cp,i}^c$   
 197 is the average travel time computed with unit porosity at the coarse scale at the  $i^{th}$  control plane, and  $n_{cp}$   
 198 is the number of control planes. This estimated effective porosity is an artificial numerical value which also  
 199 compensates for the loss of information in the upscaling process. This need of upscaling the porosity to  
 200 preserve the mean travel times is also reported by Zhang [60] and Fernàndez-Garcia et al. [18].

201 For each block, once the particle residence time distribution has been obtained numerically, the model-  
 202 independent nonlinear parameter estimation program, PEST [14], is used to determine the best set of mass  
 203 transfer parameters in equation (9) that matches the distribution  $F_\tau(\tau)$ . For this purpose, a penalty function  
 204 is established as follows:

$$P(\Theta) = \xi_1[\bar{\tau} - \bar{\tau}^*(\Theta)]^2 + \xi_2[\sigma_\tau^2 - \sigma_\tau^{*2}(\Theta)]^2 + \sum_{i=1}^{n_q} \omega_i [F_\tau(\tau_i) - F_\tau^*(\tau_i, \Theta)]^2 \quad (15)$$

205 where  $\Theta$  represents a vector with the transport parameters being estimated (we have noted explicitly the  
 206 dependence of the distribution function on  $\Theta$ ),  $\bar{\tau}$  is the average residence time computed from the particle  
 207 distribution,  $\bar{\tau}^*(\Theta)$  is the average residence time of  $F_\tau^*(\tau)$ , which can be derived from equation (9) as [36, 18]:

$$\bar{\tau}^*(\Theta) = \frac{L_b}{v_m}(1 + \beta) \quad (16)$$

208  $\sigma_\tau^2$  is the variance of residence time computed from the particle distribution,  $\sigma_\tau^{*2}(\Theta)$  is the variance of the

209 distribution, which can be derived from equation (9) as:

$$\sigma_{\tau}^*(\Theta)^2 = \frac{2D_{\ell}^c}{v_m^3}(1 + \beta)^2 L_b + \frac{2L_b}{v_m}\beta \int_0^{\infty} \frac{f(\alpha)}{\alpha} d\alpha \quad (17)$$

210  $n_q$  is the number of particles that travel through the block, and  $\xi_1$ ,  $\xi_2$  and  $\omega_i$  are weight coefficients, which  
 211 in this case are all set to 1.

212 The PEST code has to evaluate multiple times expression (9) for different sets of the mass transfer  
 213 coefficients being determined; for this purpose we have used the code STAMMT-L [29].

### 214 3. Numerical Evaluation

#### 215 3.1. Model Configuration

216 Consider a synthetic three-dimensional confined aquifer under a uniform, natural-gradient flow condition,  
 217 as shown in Figure 1, it will be the reference. A set of 30 hydraulic conductivity fields was generated using  
 218 the code GCOSIM3D [22]. The field is parallelepipedic with dimensions of  $x = 200$  m,  $y = 140$  m, and  $z = 70$   
 219 m and a discretization of  $\Delta x = \Delta y = \Delta z = 1$  m. Only the inner domain consisting of  $180 \times 120 \times 60$  cells  
 220 will be uniformly upscaled to  $18 \times 12 \times 12$  blocks, resulting in an overall scale-up factor of 500. The following  
 221 standardized exponential semivariogram was used for the simulation of the isotropic hydraulic conductivity  
 222 field:

$$\frac{\gamma_x(r)}{\sigma_x^2} = 1 - \exp\left[-\frac{r}{\lambda_x}\right] \quad (18)$$

223 where  $\lambda_x [L]$  is the range with a value of 12 m in all the directions and  $r [L]$  is the directional lag distance.  
 224 The variance  $\sigma_x^2$  of the natural logarithm of hydraulic conductivity is 4.0 (similar to the one found, for  
 225 instance, at the MADE site [40]), to represent highly heterogeneous media. The aquifer was modeled with  
 226 constant head boundaries at  $x = 0$  m and  $x = 180$  m and with no-flow boundaries at the remaining model  
 227 faces. The average hydraulic gradient induced by the constant head boundaries is 0.01. The porosity is  
 228 assumed constant and equal to 0.3.

229 At the fine scale, the five-point block-centered finite-difference groundwater flow model MODFLOW  
 230 2000 [30] was employed to solve the flow equation (1). The interface velocities were calculated, and then  
 231 utilized in the random walk particle tracking code RW3D [17, 46], which was used to solve the fine scale  
 232 transport equation (2). In this approach, the evolution in time of each particle is comprised of a deterministic  
 233 component, which depends only on the local velocity field, and a superposed Brownian motion responsible  
 234 for dispersion. A hybrid scheme is used for the velocity interpolation which provides local as well as global

235 divergence-free velocity fields within the solution domain. Meanwhile, a continuous dispersion tensor field  
 236 provides good mass balance at grid interfaces of adjacent cells with contrasting hydraulic conductivities  
 237 [35, 46]. Furthermore, in contrast to the common constant-time scheme used in random walk modeling, a  
 238 constant-displacement scheme [56], which modifies automatically the time step size for each particle according  
 239 to the local velocity, is employed in order to decrease computational effort.

240 At the coarse scale, the nineteen-point block-centered finite-difference groundwater model FLOWXYZ [38]  
 241 was employed to solve the flow equation (4). The most remarkable characteristic of this forward flow simulator  
 242 is the capacity to deal with full conductivity tensors defined at block interfaces. Hydraulic conductivity  
 243 tensors are defined at the block interfaces eliminating the need to average conductivity tensors at adjacent  
 244 blocks to approximate their values at the interfaces. This scheme has been shown to perform better than  
 245 the MODFLOW LVDA package [38], and has been successfully applied in other studies [e.g., 62, 37]. Again,  
 246 the RW3D was used to solve the coarse scale multi-rate transport equation (5) based on the methodology  
 247 presented by Salamon et al. [45]. Mass transfer processes are efficiently incorporated into the particle tracking  
 248 algorithm by switching the state of the particle between mobile/immobile states according to appropriate  
 249 transition probabilities.

250 For the sake of simplicity, we neglect dispersion, and only consider advection, at the fine scale, i.e.,  
 251  $D_m = 0$  and  $\alpha_i = 0$ . A total of 20000 particles (a number that we have tested yields stable transport  
 252 predictions for this specific case) randomly distributed in a rectangular-shaped area of 60 m width and 30  
 253 m height located orthogonal to the principal flow direction in the plane at  $x = 20$  m were released at time  
 254  $t = 0$ . The variable time step was computed on the basis of a grid Courant number of 0.01. A unit mass  
 255 was assigned to each particle. Control planes are located within the aquifer to measure the mass arrival at  
 256 10 m intervals (see Figure 2).

Figure 1: A realization of reference lnK field ( $\sigma_{lnK}^2=4.0$ ) overlaid with the discretization of the numerical model at the coarse scale.

### 257 3.2. Flow upscaling results

258 Prior to transport upscaling we wish to demonstrate the effectiveness and robustness of the interblock  
 259 Laplacian-with-skin approach to flow upscaling as compared with other methods, such as the block-centered

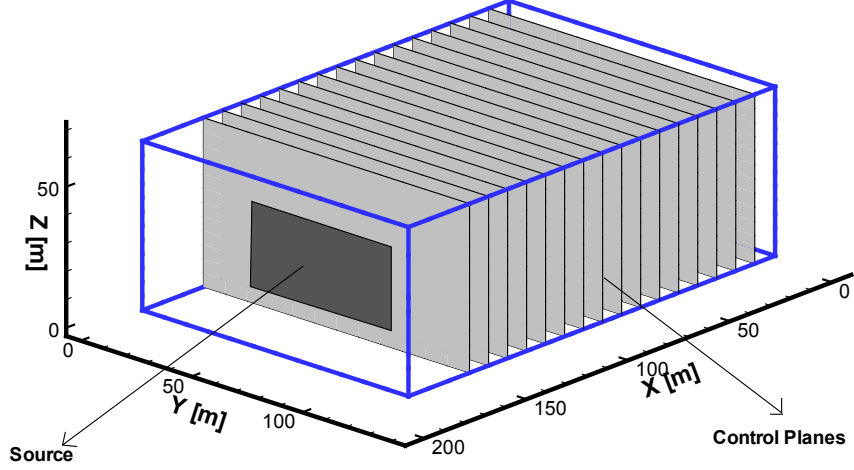


Figure 2: Sketch of transport simulations. The shaded rectangle located in the upstream zone delineates the initial particle injection zone. Control planes are also shown for measuring the mass fluxes.

260 simple-Laplacian approach, the interblock-centered simple-Laplacian approach, and the Landau-Lifshitz-  
 261 Matheron conjecture for 3D isotropic media [41]. For this purpose a single realization is analyzed. Our  
 262 goal, as that of any upscaling exercise, is to generate a heterogeneous coarse model which predicts the  
 263 interblock flows as close as possible to those derived from a fine scale simulation. We will focus on interblock  
 264 flow reproduction and disregard the analysis of piezometric heads, since the errors in piezometric head  
 265 reproduction are always much smaller.

266 We compare the coarse scale flows obtained after solving the flow equation with the upscaled conductivi-  
 267 ties, with the reference flows obtained from the solution of the flow equation at the fine scale. The mismatch  
 268 between these two values is measured by a Relative Bias defined as:

$$RB = \left( \frac{1}{N} \sum_N \frac{|q_x^f - q_x^c|}{q_x^f} \right) \cdot 100, \quad (19)$$

269 where  $N$  is the number of interblocks used to compute the relative bias;  $q_x^f$  is the specific discharge computed  
 270 on the fine scale solution, and  $q_x^c$  represents the specific discharge from the coarse scale simulation. Because  
 271 the  $x$  flow direction plays an important role in this case, the flow comparisons mainly focus on this direction.  
 272 Similar results (not displayed) are obtained for the orthogonal directions. Also, as noted by Vermeulen et al.  
 273 [54], the boundary conditions have an impact on the performance of upscaling for the nearby blocks, for  
 274 this reason, and in order to filter out this impact in the comparison of the different methods, only the inner  
 275  $14 \times 8 \times 10$  blocks are used to calculate the relative bias.

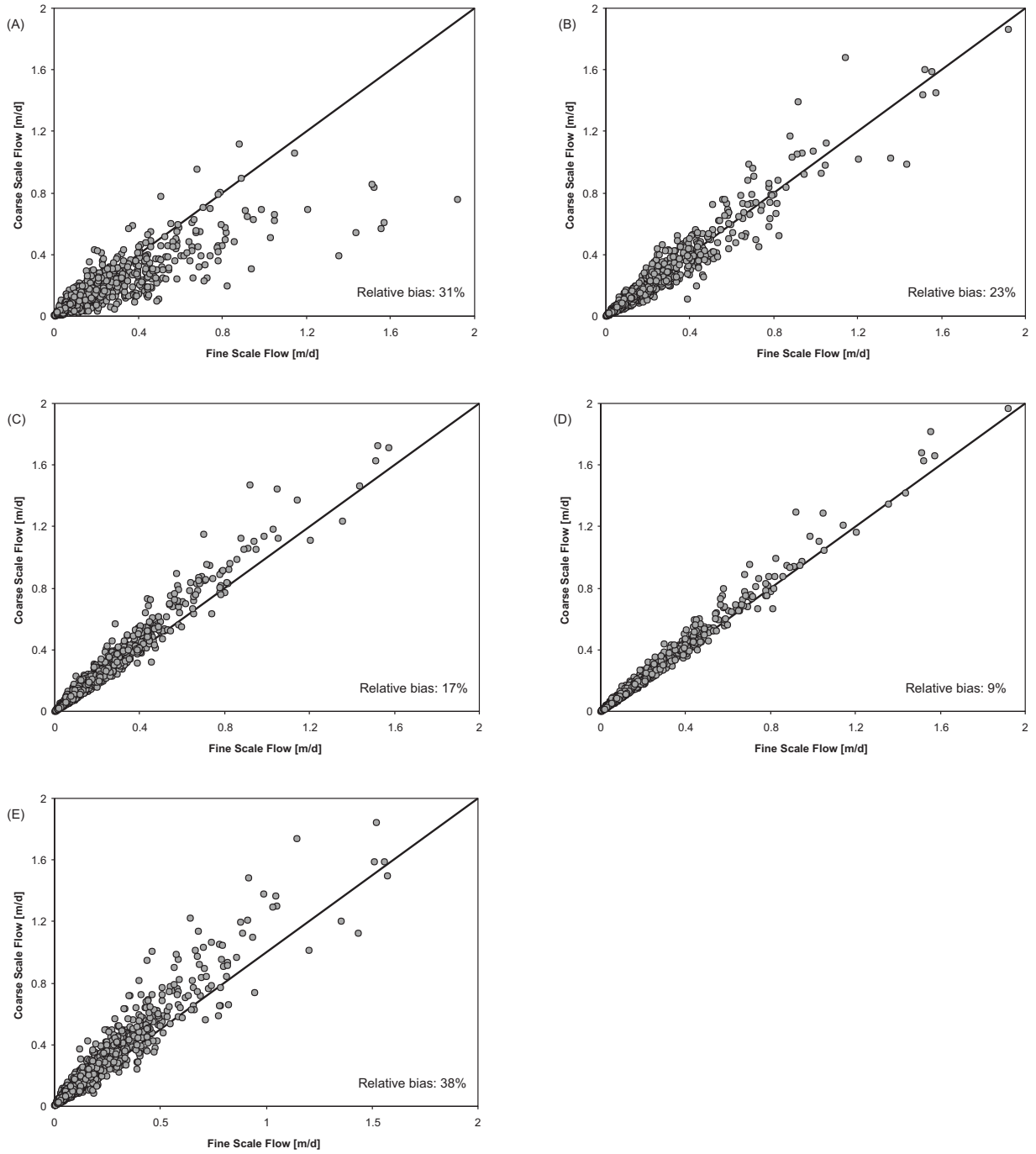


Figure 3: Flow comparisons at the fine and coarse scales on a single realization. (A) the block-centered simple-Laplacian method; (B) the interblock-centered simple-Laplacian method; (C) the interblock-centered full-tensor Laplacian-with-skin (skin size 3 m); (D) the interblock Laplacian-with-skin (skin size: 10 m along rows, 10 m along columns and 5 m along layers); (E) Landau-Lifshitz-Matheron conjecture for 3D isotropic media.

276 Figure 3 shows the cross-plots between the flows computed on the fine scale (reference values) and the  
 277 ones computed on the coarse scale for several upscaling approaches. Results indicate: (1) interblock upscaling  
 278 is better than block-centered upscaling, since it avoids the additional averaging process within the coarse  
 279 flow simulator needed to approximate the interblock values (31% relative bias using block-centered simple-  
 280 Laplacian to 23% relative bias using interblock-centered simple-Laplacian, see Figures 3A and 3B). This  
 281 result agrees with previous finding [38]. (2) Compared with the simple-Laplacian method, the Laplacian-  
 282 with-skin significantly improves the coarse scale results (23% relative bias using interblock simple-Laplacian  
 283 to 9% relative bias using interblock Laplacian-with-skin, see Figure 3B and 3D); the main reasons for these  
 284 results are the use of a full hydraulic conductivity tensor to represent the interblock property and the use  
 285 of a skin to approximate the “real” boundary conditions around the interblock, in contrast with the simple-  
 286 Laplacian approach which seeks a diagonal hydraulic conductivity tensor with boundary conditions directly  
 287 at the block sides. (3) The significance of the skin size is evident as it was already pointed out by Zhou et al.  
 288 [62] (17% relative bias using interblock Laplacian with a skin size of 3 m, down to 9% relative bias using  
 289 interblock Laplacian with a skin of 10 m in the  $x$  and  $y$  directions and 5 m in the  $z$  direction, see Figures  
 290 3C and 3D). The high variance of hydraulic conductivity, as is the case in this example with  $\sigma_{lnk}^2=4.0$ , can  
 291 result in local flows departing significantly from the average flow direction (along the  $x$  axis in this case), in  
 292 which case the use of a full tensor and the skin size is more important. (4) For a mild isotropic heterogeneous  
 293 field, the Landau-Lifshitz-Matheron conjecture (a close expression that gives the upscaled conductivity as a  
 294  $p$ -norm of the fine scale conductivities within the block, in which  $p$  only depends on the dimensionality of the  
 295 problem) performs well [12]. However, when the global variance increases, the conjecture loses its accuracy  
 296 and it is better to resort to the numerical flow experiments as is the case here, i.e., the Laplacian-with-skin  
 297 method (38% relative bias using conjecture to 9% relative bias using interblock Laplacian-with-skin of 10 m  
 298 along rows, 10 m along columns and 5 m along layers), see Figure 3D and 3E).

299 In short, the best reproduction of the fine scale flows is given by the interblock-centered Laplacian-with-  
 300 skin approach. This scheme is retained for the subsequent transport upscaling.

### 301 3.3. Transport upscaling results

302 We examined two transport upscaling approaches using the same set of upscaled hydraulic conductivities  
 303 obtained in section 3.2; in the first one, we only model advection using the velocities from the coarse scale  
 304 flow simulation, and in the second one, we include the multi-rate term in the transport equation at the coarse  
 305 scale and perform transport upscaling to determine enhanced macrodispersion coefficients, upscaled effective  
 306 porosities and the parameters of the multi-rate transfer model. The multi-rate model estimates the mass

307 transfer parameters as described in section 2.3. It should be noted that we do not make the comparison  
 308 with an intermediate model including only enhanced macrodispersion coefficients, since it has already been  
 309 shown [e.g., 64, 16, 20, 59, 18] that upscaled macrodispersion coefficients are not sufficient to reproduce the  
 310 transport behavior for highly heterogeneous media.

311 As mentioned previously, the synthetic studies of Fernàndez-Garcia et al. [18] have shown that the double-  
 312 rate mass transfer model is better than the single-rate model in 2D mass transport upscaling. Herein, we  
 313 only consider the double-rate mass transfer model to represent the mass transfer process, i.e., in each coarse  
 314 block, the solute transport is assumed to happen in three zones: transport in the mobile zone is mainly by  
 315 advection, while transport in the other two immobile zones is by diffusion-like processes.

316 With regard to the double-rate mass transfer model, the mass transfer rate density function  $f(\alpha)$  and  
 317 the memory function  $g(t)$  are:

$$\begin{aligned}
 f(\alpha) &= \frac{\beta_1}{\beta} \delta(\alpha - \alpha_1) + \frac{\beta_2}{\beta} \delta(\alpha - \alpha_2) \\
 g(t) &= \alpha_1 \frac{\beta_1}{\beta} e^{-\alpha_1 t} + \alpha_2 \frac{\beta_2}{\beta} e^{-\alpha_2 t}
 \end{aligned}
 \tag{20}$$

318 Accordingly, the parameters being estimated, are collected as a vector in  $\Theta = [\alpha_1, \alpha_2, \beta_1, \beta_2, A_l]$ . Notice  
 319 that the parameters are spatially variable since they are estimated for each upscaled block independently.

320 We compare the effectiveness of the transport upscaling by analyzing the breakthrough curves at different  
 321 control planes in one specific realization and by looking at the ensemble results. For the ensemble results we  
 322 will look at the early (5<sup>th</sup> percentile of the BTC), median (50<sup>th</sup> percentile) and late (95<sup>th</sup> percentile) travel  
 323 times.

324 Results using the advective-only model and the double-rate transport model are shown (see Figure 4 for  
 325 the reproduction of BTCs in one realization and Figure 5 for the ensemble behavior of early, median and late  
 326 travel times). From these results, we see that: (1) In contrast to the advective-only model, the double-rate  
 327 mass transfer upscale model displays a higher accuracy to reproduce the fine scale breakthrough curves, in  
 328 particular, the late travel times. Therefore, it is important to include the fictitious mass transfer process  
 329 for solute transport predictions after upscaling. (2) In agreement with the study of Fernàndez-Garcia and  
 330 Gómez-Hernández [16], it is shown that the advective-only model even when using a sophisticated hydraulic  
 331 conductivity upscaling (interblock Laplacian-with-skin here) can result in overestimating the early travel  
 332 times and underestimating the late travel times in very heterogeneous media. (3) The small deviations in  
 333 the reproduction of the BTCs by the mass transfer model may be due to fact that the upscaled mass transfer  
 334 parameters are derived from a one-dimensional analytical solution of the double-rate transport model (see

335 Equation (9)).

### 336 *3.4. Propagation of Uncertainty*

337 Due to the inherent lack of information in groundwater modeling, an uncertainty assessment is commonly  
338 requested in solute transport simulations [e.g., 47, 42]. Quantifying the uncertainty associated with flow and  
339 transport modeling should be important for the decision maker to assess the degree of confidence of his  
340 decisions. Here, we have analyzed how the uncertainty is estimated from the ensemble of realizations at the  
341 fine scale and after flow and transport upscaling. We will analyze the propagation of uncertainty through  
342 the upscaling process, along the same line as Fernàndez-Garcia and Gómez-Hernández [16].

343 The use of 30 realizations may seem a small number to perform an uncertainty evaluation in such a  
344 heterogeneous aquifer. However, our purpose is not so much to analyze the number of realizations needed  
345 to obtain a good estimation of model uncertainty, but rather to compare the uncertainty derived from 30  
346 realizations, before and after upscaling. If uncertainty upscales well for 30 realizations, it should do so for a  
347 larger number of realizations.

348 We evaluate uncertainty by calculating the spread in the ensemble of cumulative breakthrough curves at  
349 all the control planes. More precisely, we quantified uncertainty by the 95% confidence interval related with  
350 the early, median, and late arrival time of particles to each control plane. The early arrival time reflects  
351 the fastest pathways between source and control plane, which is for example of importance for the safety  
352 assessment of nuclear waste repositories. The late arrival time constitutes important information for the  
353 calculation, for example, of clean-up times in contaminated aquifer remediation.

354 The evolution of uncertainty with the travel distance is shown in Figure 6. We can see that: (1) For  
355 the early arrival time, the advection-only model and double-rate mass transfer model show a slight overes-  
356 timation of the uncertainty. (2) For the median arrival time, the double-rate mass transfer model is better  
357 in reproducing the uncertainty estimated at the fine scale than the advective-only model. (3) For the late  
358 time, it is evident that the use of double-rate mass transfer model clearly outperforms the advective-only  
359 for distances larger than 60 m, and less clearly (because of the scale the results are plotted) for the shorter  
360 distances.

361 In highly heterogeneous formulations, hydraulic conductivity upscaling is not sufficient to preserve the  
362 uncertainty. Transport upscaling, through the use of a mass transfer process at the coarse scale is needed  
363 for proper upscaling of the uncertainty associated with solute transport predictions.



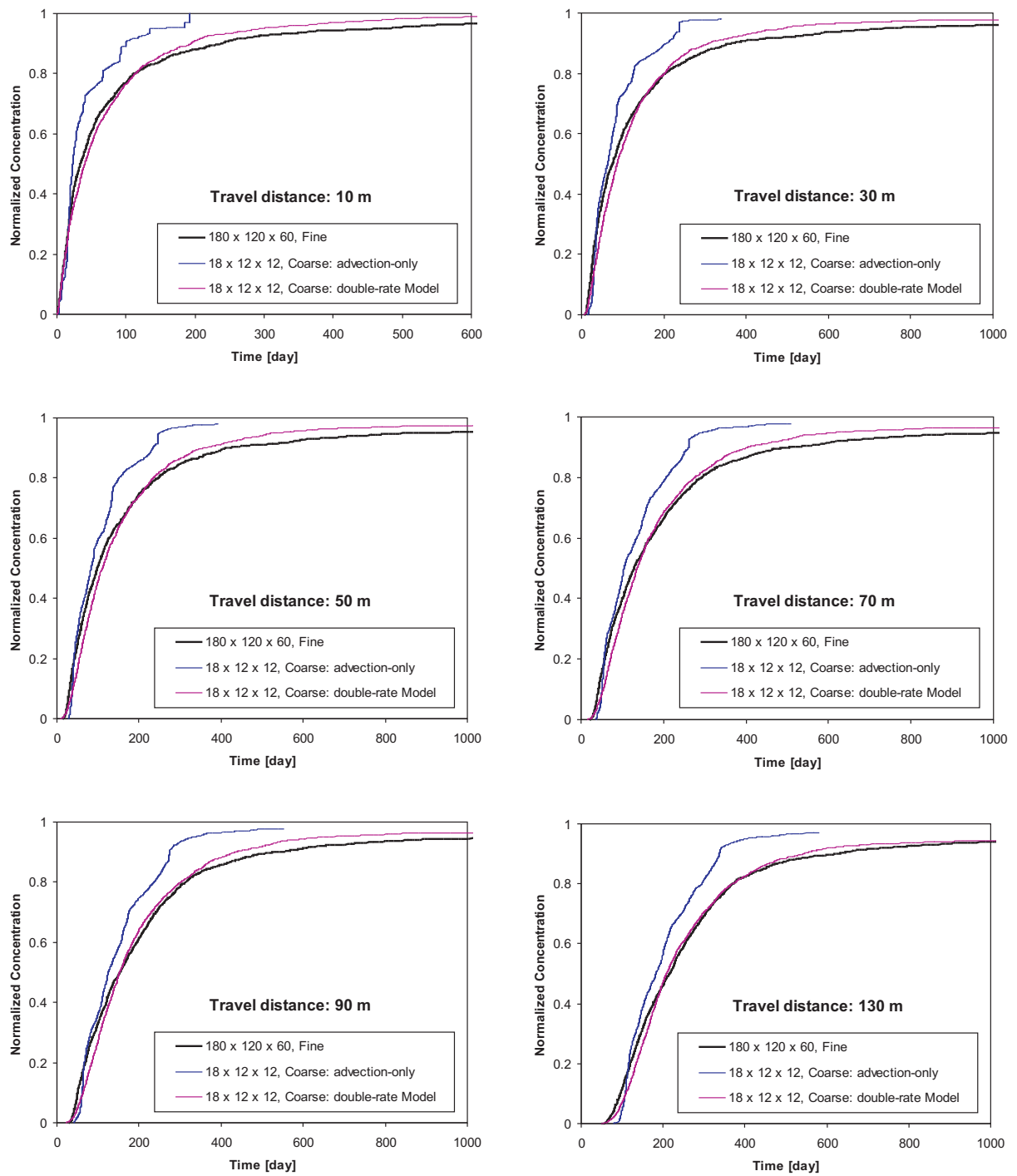


Figure 4: Comparison of fine scale cumulative breakthrough curves with those obtained by the upscaled transport models at six different control planes.

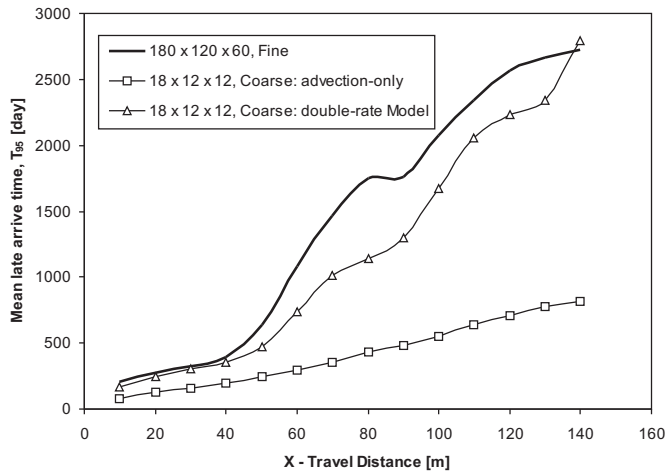
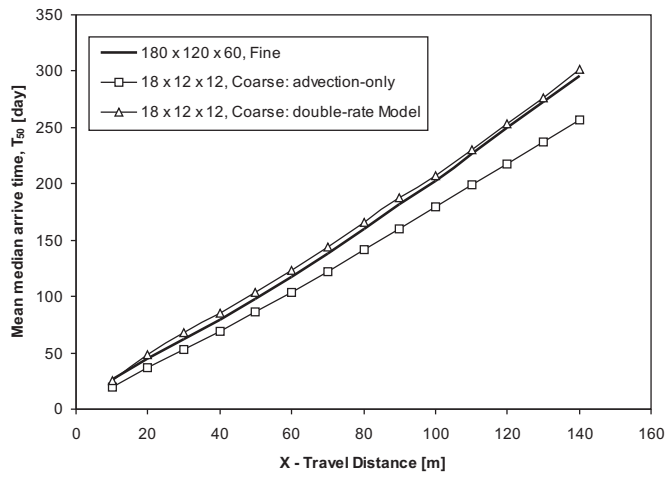
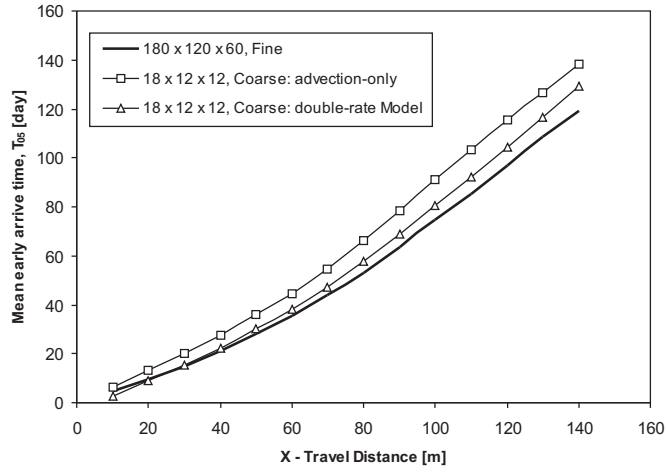


Figure 5: Ensemble travel times (early, median, and late travel times) as a function of travel distance, and comparison of the fine scale simulations to the upscaled simulations.

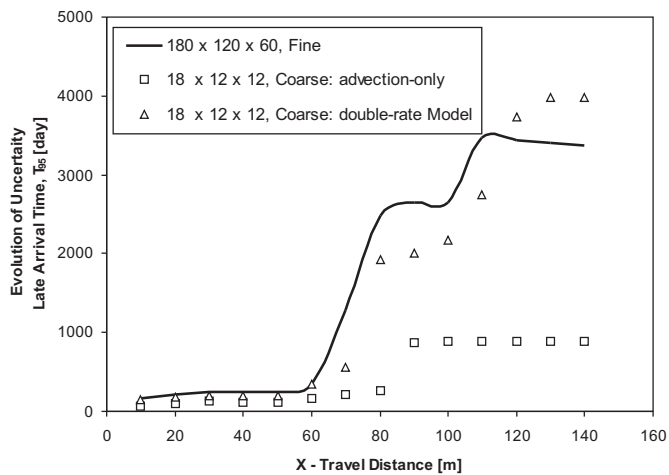
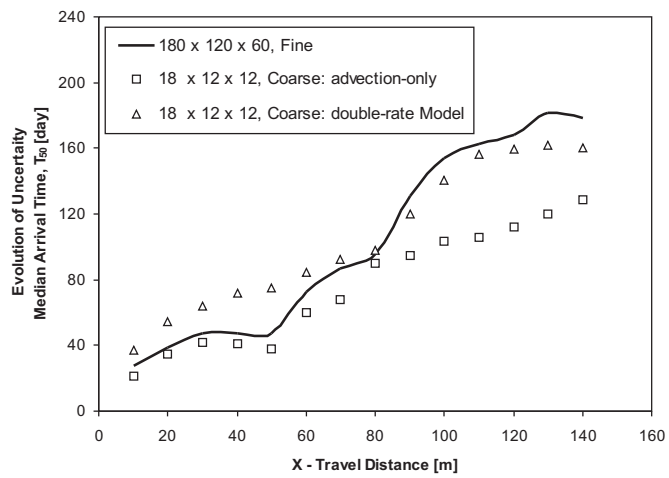
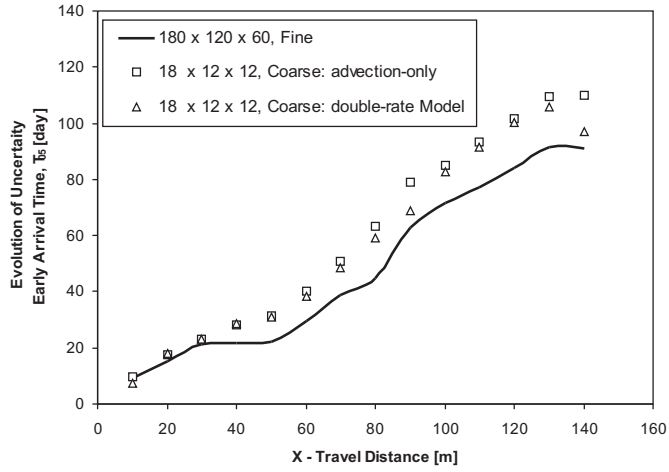


Figure 6: Evolution of uncertainty as a function of travel distance for the early, median, and late travel times, as measured by the width of the 95% confidence interval derived from an ensemble of 30 realizations. Calculations were performed at the fine scale, and at the coarse scale for two different upscaling approaches.

#### 364 4. Discussion

365 We have presented and demonstrated an algorithm for transport upscaling to reduce the computational  
366 burden of transport predictions in three-dimensional highly heterogeneous media. But, how general is the  
367 algorithm? Will it work for different case studies? Will it work for different transport experiments? Although  
368 we recognize that the results obtained are specific to the case study under consideration, we believe that the  
369 upscaling procedure is general and it should work for other settings, as discussed below.

370 We present the results for statistically isotropic fine scale conductivities. What if the fine scale conduc-  
371 tivities had been statistically anisotropic, with a much larger correlation length in the horizontal plane than  
372 in the vertical direction? What if the fine scale conductivities display curvilinear features, such as those  
373 associated with channels? In the case of statistical anisotropy, it would be necessary to adjust the size of the  
374 coarse blocks proportionally to the correlation lengths in each direction, in order to reduce the amount of  
375 smoothing in the directions of shortest continuity. In the case of curvilinear features, the proposed approach  
376 will yield upscaled conductivity tensors, the principal directions of which will change from block to block,  
377 inducing fluid velocities in the coarse model following those curvilinear features. The proposed approach  
378 has no problem in dealing with hydraulic conductivity tensors with arbitrary orientations of their principal  
379 directions. The block-by-block upscaling procedure is local, each block is isolated and a local flow exercise is  
380 performed in each block; at this local scale, the anisotropic correlation or the curvilinear features should not  
381 be clearly distinguishable from the intrinsic heterogeneity of the fine scale conductivities within the block;  
382 therefore, the upscaling algorithm should perform similarly. The question, remained to be answered, is  
383 whether when the blocks are assembled they will capture the global behavior of the statistically anisotropic  
384 formation or of the curvilinear features, or some specific corrections have to applied in these cases.

385 We present an analysis for a confined aquifer under steady-state flow conditions. We have not investigated  
386 how the upscaled coarse model would behave under transient conditions. We conjecture that the upscaled  
387 model should reproduce the the transient flow response of the the fine scale model with a degree of accuracy  
388 similar to the one obtained here for steady-state conditions, since the upscaled block conductivities are  
389 determined using different flow configurations applied to the block being upscaled. However, the upscaled  
390 transport parameters are based on the particle residence times for a specific velocity field; since, for transient  
391 flow conditions, the velocity field changes with time, it should be further investigated how much the upscaled  
392 transport parameters change as the velocity field changes, and decide whether these transport parameters  
393 should be made time dependent or there is a set of optimal parameters that would work well for the entire  
394 transient period. Also, in the case of transient flow, the need to upscale the storage coefficient needs to

395 be addressed. Regarding the application of this approach for an unconfined aquifer, the general upscaling  
396 procedure should remain the same, all blocks should be upscaled as if they were fully saturated, and then,  
397 special caution should be taken in the numerical simulation model to account for those cells intersected by  
398 the phreatic surface at the time of computing the mass balances involving those cells. We have not analyzed  
399 this case because we do not have a numerical flow simulator capable of using full conductivity tensors and  
400 accounting for a phreatic surface.

401 The issue of how the upscaled transport parameters will perform under transient conditions (i.e., different  
402 velocity fields in time), brings the question of what will happen if the flow geometry changes substantially  
403 with respect to that for which the parameters were computed. A priori, we anticipate that the transport  
404 parameters would have to be recomputed, since the flow velocity field will change, and so will the residence  
405 times in the blocks.

406 We present a sequential upscaling procedure in which first, we compute the upscaled flow parameters,  
407 and then we use these parameters to compute the upscaled transport parameters. However, if the final aim  
408 of our analysis were to get the best transport predictions at the coarse scale, even compromising the accuracy  
409 of flow reproduction, we could think of performing the flow and transport upscaling jointly, therefore using  
410 the particle residence times within the block being upscaled in the computation of the coarse conductivity  
411 tensors. This is an interesting avenue of research that has not been investigated in this paper.

412 We have used a homogeneous porosity throughout the exercise. If porosity had been heterogeneous it  
413 would have had to be upscaled, too

414 There are two main drawbacks in the proposed method: the need to use the particle residence times  
415 obtained after a simulation of the flow and transport equations at the fine scale, and the need to correct the  
416 porosity at the coarse scale, even though the porosity is homogenous at the fine scale.

417 The first drawback beats, in principle, the whole purpose of upscaling, which is to avoid having to  
418 simulate flow and/or transport at the fine scale. For this reason, this paper loses some of its practicality,  
419 and could be justified (from a practical point of view) only if the upscaled model is to be used for a more  
420 complex type of modeling (i.e. reactive transport) avoiding the need to run the complex model at the fine  
421 scale. In order not to have to obtain the fine scale solution for the transport upscaling, we have tried to  
422 follow the same local approach as for the flow upscaling, that is, to isolate the block plus a sufficiently large  
423 skin and to solve local transport problems for several boundary conditions, and then derive the upscaled  
424 transport parameters; however, we have not succeeded with this approach, which has always resulted in  
425 biased transport predictions. There is, therefore, additional research needed in the transport upscaling

426 procedure in order to yield it more practical. Our contribution with this paper is to demonstrate that, in 3D  
427 modeling of flow and transport, it is possible to systematically derive flow and transport upscaled parameters  
428 as long as we acknowledge that removing the heterogeneity within the block implies turning conductivities  
429 into tensors and including an enhanced macrodispersion and a mass transfer process for the solute transport.

430 The second drawback requires further investigation. We are not the first ones to face the need to make this  
431 adjustment for the coarse scale porosity [64, 60, 18]. The need for this correction is due to the accumulation  
432 of small biases in the transport modeling for each coarse block. When the transport parameters of each  
433 coarse block are computed, they are determined trying to reproduce the particle residence time distribution  
434 within the block with emphasis in matching the mean residence time; however, there seems to be a small  
435 systematic bias in this determination, which, at the end, forces us to correct the coarse porosities so that  
436 the breakthrough curves from the upscaled model are not shifted with respect to those from the fine scale  
437 model.

438 There is a need to know the fine scale parameters over the entire aquifer. Obviously, these parameter  
439 values will never be available, they have to be generated on the basis of available data. The issue of scales has  
440 been discussed for many years in the literature; it is a very old issue (known as the change of support problem)  
441 in mining [34], and a little bit more recent in hydrogeology and petroleum engineering; a good paper on the  
442 subject from the hydrogeology literature is the one by [10], in which Dagan talks about measurement and  
443 model scales, among other scales. For many years, data were measured, and without further consideration  
444 they were used to inform the parameter values of the groundwater flow model elements, until a concern  
445 about the so called “missing scale” was risen, mostly in the petroleum literature [52, 53], and the need to  
446 account for the disparity of scales between measurements and model cells was recognized [21]. Data are  
447 collected at a scale, generally, much smaller than the scale at which models are going to be discretized. Data  
448 spatial variability can be characterized at such scale by standard geostatistical methods [13] or by the more  
449 powerful and sophisticated multipoint geostatistical approaches [51], and this characterization can be used to  
450 generate conditional realizations, at the sampling scale, over discretized grids of multi-million cells. It is not  
451 proper to characterize the sampled data and use them directly for the generation of realizations at a larger  
452 scale suitable for numerical modeling, since the spatial variability patterns of the “equivalent” properties  
453 that should inform the larger blocks are completely different from that of the sampled data. Besides, as we  
454 have shown, for the purpose of transport modeling, removing the within-block heterogeneity requires the  
455 introduction of additional processes to make up for this loss of variability, which makes virtually impossible  
456 to generate the additional parameters directly from a few sampled data. As proposed in this, and many other

457 papers on upscaling, the proper way to account for the disparity of scales is to build fine scale models based  
458 on the data, then to upscale them so that the model size is amenable to numerical modeling. It remains  
459 open the problem of how to integrate sampled data taken at different scales.

460 We recognize that the results have been demonstrated in a single case study, but we conjecture that  
461 the good performance of the method proposed is not case specific, and we base this conjecture in that  
462 the upscaling exercise is performed on a block by block basis at a scale in which the specific features of the  
463 different case studies will be less noticeable. We had to upscale several thousands of blocks using a systematic  
464 approach, with each block having a different distribution of fine scale conductivities. The upscaled parameters  
465 would have been computed similarly had the flow geometry or the conductivity heterogeneity changed. We  
466 acknowledge that the final results we present are based on the assembly of these blocks for a specific flow  
467 and transport problem, and the performance of this final assembly for a different case study may not work  
468 so well as it did in our example.

469 Further research is needed (i) to avoid the solution of the flow and transport at the fine scale in order  
470 to determine the coarse scale transport parameters, (ii) to explain the need for correcting the porosity when  
471 moving from the fine to the coarse scale, (iii) to determine how to upscale heterogeneous porosities, (iv)  
472 to evaluate the approach for different conditions/scenarios, such as statistical anisotropic conductivities,  
473 transient flow conditions or radial flow and (v) to account for data measured at different scales.

## 474 5. Summary and Conclusions

475 We have presented and demonstrated an algorithm for transport upscaling in three-dimensional highly  
476 heterogeneous media. This work is an extension of the work by Fernández-García et al. [18] in two dimensions.  
477 Some of the critical features of this method is that it uses an elaborated Laplacian-with-skin approach to  
478 reproduce the flows instead of the simple-Laplacian scheme, the use of a multi-rate mass transfer process  
479 at the coarse scale to compensate for the loss of information during upscaling, and the need to perform a  
480 piecewise upscaling of effective porosity.

481 We have used a synthetic example to demonstrate the advantages of the interblock Laplacian-with-skin  
482 approach to upscale hydraulic conductivities as compared with other approaches. We found that using  
483 interblock centered conductivities and that using a skin to compute them results in a good reproduction of  
484 flows at the fine scale.

485 Moreover, we found that proper transport upscaling is particularly important for the reproduction of  
486 the late time behavior of the solute breakthrough curves. We also found that proper transport upscaling is

487 important to not underestimate the breakthrough curve prediction uncertainty.

488 **Acknowledgements** The authors gratefully acknowledge the financial support by ENRESA (project  
489 0079000029) and the European Commission (project PAMINA). The second author also acknowledges the  
490 financial support from China Scholarship Council (CSC). We also wish to acknowledge Dr.Llerar-Meza  
491 Gerónimo (Autonomous University of Chihuahua, Mexico) for his input to this paper. We also wish to  
492 thank the comments of the six reviewers, which helped improving the final version of the manuscript.

## 493 **References**

- 494 [1] Bear, J., 1972. Dynamics of fluids in porous media. American Elsevier Pub. Co., New York.
- 495 [2] Benson, D. A., Wheatcraft, S. W., Meerschaert, M. M., 2000. Application of a fractional advection-  
496 dispersion equation. *Water Resour Res* 36 (6), 1403–1412.
- 497 [3] Berkowitz, B., Scher, H., 1998. Theory of anomalous chemical transport in random fracture networks.  
498 *Phys Rev E* 57 (5), 5858–5869.
- 499 [4] Bierkens, M., Gaast, J., 1998. Upscaling hydraulic conductivity: theory and examples from geohydro-  
500 logical studies. *Nutrient Cycling in Agroecosystems* 50, 193–207.
- 501 [5] Burnett, R. D., Frind, E. O., 1987. Simulation of contaminant transport in three dimensions: 2. dimen-  
502 sionality effects. *Water Resour Res* 23 (4).
- 503 [6] Carrera, J., Sánchez-Vila, X., Benet, I., Medina, A., Galarza, G., Guimera, J., 1998. On matrix diffusion:  
504 formulations, solution methods and qualitative effects. *Hydrogeol J* 6 (1), 178–190.
- 505 [7] Cassiraga, E. F., Fernández-García, D., Gómez-Hernández, J. J., 2005. Performance assessment of solute  
506 transport upscaling methods in the context of nuclear waste disposal. *Int J of Rock Mec Min* 42 (5-6),  
507 756–764.
- 508 [8] Chen, Y., Durlafsky, L. J., Gerritsen, M., Wen, X. H., 2003. A coupled local-global upscaling approach  
509 for simulating flow in highly heterogeneous formations. *Adv. Water Resour.* 26 (10), 1041–1060.
- 510 [9] Cushman, J. H., 1984. On unifying the concepts of scale, instrumentation, and stochastics in the devel-  
511 opment of multiphase transport theory. *Water Resour. Res.* 20 (11), 1668–1676.
- 512 URL <http://dx.doi.org/10.1029/WR020i011p01668>



- 513 [10] Dagan, G., 1986. Statistical theory of groundwater flow and transport: Pore to laboratory, laboratory  
514 to formation, and formation to regional scale. *Water Resour. Res.* 22 (9), 120S–134S.
- 515 [11] Dagan, G., 1994. Upscaling of dispersion coefficients in transport through heterogeneous formations.  
516 *Computational Methods in Water Resources X* 1, 431–439.
- 517 [12] Desbarats, A. J., 1992. Spatial averaging of hydraulic conductivity in three-dimensional heterogeneous  
518 porous media. *Math. Geol.* 24 (3), 249–267.
- 519 [13] Deutsch, C. V., Journel, A. G., 1992. *GSLIB, Geostatistical Software Library and User’s Guide*. Oxford  
520 University Press, New York.
- 521 [14] Doherty, J., 2004. *PEST model-independent parameter estimation, user manual*. Watermark Numerical  
522 Computing, Brisbane, Australia, 3349.
- 523 [15] Feehley, C. E., Zheng, C., Molz, F. J., 2000. A dual-domain mass transfer approach for modeling  
524 solute transport in heterogeneous aquifers: Application to the macrodispersion experiment (MADE)  
525 site. *Water Resour Res* 36 (9), 2501–2515.
- 526 [16] Fernàndez-Garcia, D., Gómez-Hernández, J. J., 2007. Impact of upscaling on solute transport: Travel-  
527 times, scale dependence of dispersivity, and propagation of uncertainty. *Water Resour Res* 43 (2).
- 528 [17] Fernàndez-Garcia, D., Illangasekare, T. H., Rajaram, H., 2005. Differences in the scale dependence of  
529 dispersivity and retardation factors estimated from forced-gradient and uniform flow tracer tests in  
530 three-dimensional physically and chemically heterogeneous porous media. *Water Resour Res* 41 (3),  
531 W03012.
- 532 [18] Fernàndez-Garcia, D., Llerar-Meza, G., Gómez-Hernández, J. J., 2009. Upscaling transport with mass  
533 transfer models: Mean behavior and propagation of uncertainty. *Water Resour Res* 45, W10411.
- 534 [19] Freeze, R. A., Cherry, J. A., 1979. *Groundwater*. Prentice-Hall.
- 535 [20] Frippiat, C. C., Holeyman, A. E., 2008. A comparative review of upscaling methods for solute transport  
536 in heterogeneous porous media. *J. of Hydrology* 362 (1-2), 150–176.
- 537 [21] Gómez-Hernández, J. J., 1991. A stochastic approach to the simulation of block conductivity values  
538 conditioned upon data measured at a smaller scale. Ph.D. thesis, Stanford University.

- 539 [22] Gómez-Hernández, J. J., Journel, A. G., 1993. Joint sequential simulation of multi-Gaussian fields.  
540 Geostatistics Troia 92 (1), 85–94.
- 541 [23] Gómez-Hernández, J. J., Rubin, Y., 1990. Spatial averaging of statistically anisotropic point conductiv-  
542 ities. In: Optimizing the Resources of Water Management. Asce, pp. 566–571.
- 543 [24] Gómez-Hernández, J. J., Wen, X. H., 1994. Probabilistic assessment of travel times in groundwater  
544 modeling. J. of Stochastic Hydrology and Hydraulics 8 (1), 19–56.
- 545 [25] Guadagnini, A., Neuman, S. P., 1999. Nonlocal and localized analyses of conditional mean steady state  
546 flow in bounded, randomly nonuniform domains: 1. theory and computational approach. Water Resour.  
547 Res. 35 (10), 2999–3018.  
548 URL <http://dx.doi.org/10.1029/1999WR900160>
- 549 [26] Guswa, A. J., Freyberg, D. L., 2002. On using the equivalent conductivity to characterize solute spread-  
550 ing in environments with low-permeability lenses. Water Resour. Res. 38 (8), 1132.  
551 URL <http://dx.doi.org/10.1029/2001WR000528>
- 552 [27] Haggerty, R., Gorelick, S. M., 1995. Multiple-rate mass transfer for modeling diffusion and surface  
553 reactions in media with pore-scale heterogeneity. Water Resour Res 31 (10).
- 554 [28] Haggerty, R., McKenna, S. A., Meigs, L. C., 2000. On the late-time behavior of tracer test breakthrough  
555 curves. Water Resour Res 36 (12).
- 556 [29] Haggerty, R., Reeves, P. C., 2002. STAMMT-L 1.0, formulation and users guide. Tech. rep., Tech. Rep.  
557 520308, Sandia National Laboratories.
- 558 [30] Harbaugh, A. W., Banta, E. R., Hill, M. C., McDonald, M. G., 2000. MODFLOW-2000, the U.S.  
559 Geological Survey modular ground-water model. U.S. Geological Survey, Branch of Information Services,  
560 Reston, VA, Denver, CO.
- 561 [31] He, C., Durlofsky, L. J., 2006. Structured flow-based gridding and upscaling for modeling subsurface  
562 flow. Adv. Water Resour. 29 (12), 1876–1892.
- 563 [32] Indelman, P., Abramovich, B., 1994. Nonlocal properties of nonuniform averaged flows in heterogeneous  
564 media. Water Resour. Res. 30 (12), 3385–3393.  
565 URL <http://dx.doi.org/10.1029/94WR01782>

- 566 [33] Journel, A. G., Deutsch, C. V., Desbarats, A. J., 1986. Power averaging for block effective permeability.  
567 SPE 15128.
- 568 [34] Journel, A. G., Huijbregts, C. J., 1978. Mining Geostatistics. Academic Press, London.
- 569 [35] LaBolle, E. M., Fogg, G. E., Tompson, A. F., 1996. Random-walk simulation of transport in hetero-  
570 geneous porous media: Local mass-conservation problem and implementation methods. *Water Resour*  
571 *Res* 32 (3), 583–593.
- 572 [36] Lawrence, A. E., Sanchez-Vila, X., Rubin, Y., 2002. Conditional moments of the breakthrough curves  
573 of kinetically sorbing solute in heterogeneous porous media using multirate mass transfer models for  
574 sorption and desorption. *Water Resour Res* 38 (11), 1248.
- 575 [37] Li, L., Zhou, H., Gómez-Hernández, J. J., 2010. A comparative study of three-dimensional hydraulic  
576 conductivity upscaling at the macrodispersion experiment (MADE) site, on columbus air force base in  
577 mississippi (USA). *J. of Hydrology* submitted.
- 578 [38] Li, L., Zhou, H., Gómez-Hernández, J. J., 2010. Steady-state groundwater flow modeling with full tensor  
579 conductivities using finite differences. *Comput Geosci*, doi:10.1016/j.cageo.2010.04.002.
- 580 [39] Neuman, S. P., Orr, S., 1993. Prediction of steady state flow in nonuniform geologic media by conditional  
581 moments: Exact nonlocal formalism, effective conductivities, and weak approximation. *Water Resour.*  
582 *Res.* 29 (2), 341–364.
- 583 [40] Rehfeldt, K. R., Boggs, J. M., Gelhar, L. W., 1992. Field study of dispersion in a heterogeneous aquifer  
584 3. geostatistical analysis of hydraulic conductivity. *Water Resour Res* 28 (12), 3309–3324.
- 585 [41] Renard, P., Marsily, G. D., 1997. Calculating equivalent permeability: A review. *Adv. Water Resour.*  
586 20 (5-6), 253–278.
- 587 [42] Riva, M., Guadagnini, A., Fernández-García, D., Sanchez-Vila, X., Ptak, T., 2008. Relative importance  
588 of geostatistical and transport models in describing heavily tailed breakthrough curves at the lauswiesen  
589 site. *J Contam Hydrol* 101 (1-4), 1–13.
- 590 [43] Rubin, Y., Gómez-Hernández, J. J., 1990. A stochastic approach to the problem of upscaling of conduc-  
591 tivity in disordered media, Theory and unconditional numerical simulations. *Water Resour. Res.* 26 (4),  
592 691–701.

- 593 [44] Rubin, Y., Sun, A., Maxwell, R., Bellin, A., 1999. The concept of block-effective macrodispersivity and  
594 a unified approach for grid-scale-and plume-scale-dependent transport. *J Fluid Mech* 395, 161–180.
- 595 [45] Salamon, P., Fernàndez-Garcia, D., Gómez-Hernández, J. J., 2006. Modeling mass transfer processes  
596 using random walk particle tracking. *Water Resour Res* 42, W11417.
- 597 [46] Salamon, P., Fernàndez-Garcia, D., Gómez-Hernández, J. J., 2006. A review and numerical assessment  
598 of the random walk particle tracking method. *J Contam Hydrol* 87 (3-4), 277–305.
- 599 [47] Salamon, P., Fernàndez-Garcia, D., Gómez-Hernández, J. J., 2007. Modeling tracer transport at the  
600 MADE site: The importance of heterogeneity. *Water Resour Res* 30 (8).
- 601 [48] Sanchez-Vila, X., Guadagnini, A., Carrera, J., 2006. Representative hydraulic conductivities in saturated  
602 groundwater flow. *Rev Geophys* 44 (3).
- 603 [49] Scheibe, T., Yabusaki, S., 1998. Scaling of flow and transport behavior in heterogeneous groundwater  
604 systems. *Adv. Water Resour.* 22 (3), 223–238.
- 605 [50] Silva, O., Carrera, J., Kumar, S., Dentz, M., Alcolea, A., Willmann, M., 2009. A general real-time  
606 formulation for multi-rate mass transfer problems. *Hydrol Earth Syst Sc* 6 (2), 2415–2449.
- 607 [51] Strebelle, S., 2002. Conditional simulation of complex geological structures using multiple-point statis-  
608 tics. *Math. Geol.* 34 (1), 1–22.
- 609 [52] Tran, T., 1995. Stochastic simulation of permeability fields and their scale-up for flow modeling. Ph.D.  
610 thesis, Stanford University, Branner Earth Sciences Library.
- 611 [53] Tran, T., 1996. The [‘]missing scale’ and direct simulation of block effective properties. *Journal of*  
612 *Hydrology* 183 (1-2), 37 – 56.
- 613 URL [http://www.sciencedirect.com/science/article/B6V6C-45Y4JBT-6/2/  
614 e6013222f0b4f32e64cbe973bf1df549](http://www.sciencedirect.com/science/article/B6V6C-45Y4JBT-6/2/e6013222f0b4f32e64cbe973bf1df549)
- 615 [54] Vermeulen, P. T. M., Stroet, C. B. M. T., Heemink, A. W., 2006. Limitations to upscaling of groundwater  
616 flow models dominated by surface water interaction. *Water Resour Res* 42 (10), W10406.
- 617 [55] Wen, X. H., Durlofsky, L. J., Chen, Y., 2005. Efficient three-dimensional implementation of local-global  
618 upscaling for reservoir simulation. In: *SPE Reservoir Simulation Symposium*.

- 619 [56] Wen, X. H., Gómez-Hernández, J. J., 1996. The constant displacement scheme for tracking particles in  
620 heterogeneous aquifers. *Groundwater* 34 (1), 135–142.
- 621 [57] Wen, X. H., Gómez-Hernández, J. J., 1996. Upscaling hydraulic conductivities: An overview. *J. of*  
622 *Hydrology* 183 (1-2), ix–xxxii.
- 623 [58] White, C. D., Horne, R. N., 1987. Computing absolute transmissibility in the presence of Fine-Scale  
624 heterogeneity. SPE 16011.
- 625 [59] Willmann, M., Carrera, J., Sánchez-Vila, X., 2008. Transport upscaling in heterogeneous aquifers: What  
626 physical parameters control memory functions? *Water Resour Res* 44 (12), W12437.
- 627 [60] Zhang, Y., 2004. Upscaling conductivity and porosity in three-dimensional heterogeneous porous media.  
628 *Chinese Sci Bull* 49 (22), 2415–2423.
- 629 [61] Zheng, C., Wang, P. P., 1999. MT3DMS: A Modular Three-Dimensional Multispecies Transport Model  
630 for Simulation of Advection, Dispersion, and Chemical Reactions of Contaminants in Groundwater  
631 Systems; Documentation and User's. ALABAMA UNIV TUSCALOOSA.
- 632 [62] Zhou, H., Li, L., Gómez-Hernández, J. J., 2010. Three-dimensional hydraulic conductivity upscaling in  
633 groundwater modelling. *Comput Geosci*, doi:10.1016/j.cageo.2010.03.008.
- 634 [63] Zijl, W., Stam, J., 1992. Modeling permeability in imperfectly layered porous media. i. deriva-  
635 tion of block-scale permeability tensor for thin grid-blocks. *Mathematical Geology* 24, 865–883,  
636 10.1007/BF00894656.  
637 URL <http://dx.doi.org/10.1007/BF00894656>
- 638 [64] Zinn, B., Harvey, C. F., 2003. When good statistical models of aquifer heterogeneity go bad: A compari-  
639 son of flow, dispersion, and mass transfer in connected and multivariate gaussian hydraulic conductivity  
640 fields. *Water Resour. Res* 39 (3), doi:10.1029/2001WR001146.